A NUMERICAL SCHEME FOR FATIGUE SIMULATION OF LAMINATED COMPOSITES USING CZM-XFEM

Rong-Can Hong[1], Ryo Higuchi[2], Tomohiro Yokozeki[3] and Takahira Aoki[4]

[1] Department of Aeronautics and Astronautics, The University of Tokyo. Email: rchong@g.ecc.u-tokyo.ac.jp
[2, 3, 4] Department of Aeronautics and Astronautics, The University of Tokyo

Abstract: A numerical method for fatigue damage accumulation in laminated composites is developed in this paper. Extended finite element method (XFEM) and cohesive element are integrated into a numerical program for fatigue fracture. In this work, XFEM and cohesive element are applied for modelling matrix cracking and delamination in CFRP laminates respectively. A fatigue model based on cohesive zone model (CZM) is also introduced into the numerical scheme. Standard DCB and ENF fatigue tests are used as the identification of parameters of the fatigue model, and simulation models of the standard tests are established for calibrating the fatigue model of pure mode. With the parameters calibrated by the benchmarks of pure mode tests, the numerical analysis of open hole tensile (OHT) test is conducted to investigate the fracture behaviours of composite laminates under cyclic loading. The delamination and in-ply cracking are all predicted in the numerical results. The progression of fatigue damage in the simulation model is consistent with previous experimental work. This study demonstrates that the proposed numerical method can correctly predict the initiation and evolution of fatigue damage under mixed mode loading. By XFEM, in-ply matrix cracking can be modelled as multiple mesh-independent path in FE model. This paper provides a convenient approach utilizing the features of XFEM for simulating fatigue cracking in composite laminates.

Keywords: extended finite element method, cohesive zone model, fatigue, CFRP, laminated composites

INTRODUCTION

Carbon fiber reinforced plastic (CFRP) materials are increasingly being used in the aircraft and space industries due to their lightweight and high strength properties, which offer significant advantages for structural applications. While CFRPs generally have a longer fatigue life compared to metallic materials, the assessment of their lifetime for long-term service has become a critical issue due to the increasing number of applications. In a seminal study by Spearing and Beaumont [1], it was demonstrated that damage in composite structures can occur at stress levels significantly below the static failure load. However, due to the complex nature of fatigue mechanisms in composites and the limited amount of related research, characterizing the fatigue evolution in CFRPs is still considered an unsolved problem [2, 3]. In addition to constitutive fatigue models, the numerical simulation of fracture behavior during fatigue accumulation in CFRPs remains a challenging topic. The primary objective of this paper is to propose a numerical framework for studying the detailed mechanisms of fatigue accumulation in CFRPs.

The cohesive zone model (CZM) has been widely utilized to predict fracture with plastic properties and evaluate damage in structures. The fundamental concepts of CZM were initially proposed by Dugdale [4] and Barenblatt [5], who suggested that the stress behavior around the crack tip resembles the yielding of metals. Building upon the concept of maximum stress, Hillerborg et al. [6] introduced a traction-displacement relationship into CZM along with fracture energy. Various versions of constitutive laws have been developed to describe CZM [7, 8]. In this paper, Geubelle and Taylor's model [7] is applied as the damage model for CFRP structures, which will be discussed further.

In fatigue analysis, CZM is often combined with various fatigue accumulation laws. The Paris law [9], initially developed for crack growth in metals, has been proven applicable to FRP materials [10, 11]. Several research studies [12–14] have been published, proposing modified versions of the Paris law to predict damage evolution under cyclic loading, utilizing cohesive elements. However, the modified Paris law assumes the existence of cracks and cannot predict crack initiation. Recognizing the limitations of the Paris law, Nojavan et al. [15] proposed a micromechanical model that considers local states of cohesive stresses and displacements to describe CZM fatigue accumulation. Okabe and Yashiro [16] also implemented a microscopic fatigue CZM to account for both delamination and in-ply cracking. An extended version of Okabe and Yashiro's model is integrated into the numerical tool in this paper.

In numerical analysis using CZM, cohesive elements are commonly employed as the primary approach due to their convenience and ease of implementation. However, the mesh of finite element (FE) models with cohesive elements relies on the crack shapes, requiring nodes to be arranged along the cracks. Consequently, if the crack path changes, remeshing becomes necessary, making the pre-processing stage complex and time-consuming. To address these limitations, extended finite element method (XFEM) [17, 18] has emerged as an effective alternative to traditional FEM. Building upon the original XFEM, Moës and Belytschko [19] proposed a CZM-combined XFEM. Nagashima and Sawada [20] developed a quasi-3D CZM-XFEM framework using a level-set method within XFEM. Higuchi et al. [21] further integrated Nagashima and Sawada's work with an elasto-plastic constitutive law for FRPs. Building upon the framework of Higuchi et al., this paper presents a numerical scheme for fatigue CZM-XFEM, utilizing a micromechanical fatigue accumulation law to model fatigue crack growth in laminated composites.

The objective of this paper is to develop a more convenient and precise numerical approach for studying fatigue crack propagation in laminated composites. The simulation framework integrates XFEM and cohesive elements to model delamination and in-ply cracking, respectively. For the fatigue accumulation law in this study, an enhanced fatigue model based on Okabe and Yashiro's model [16] is utilized. A numerical example of fatigue open hole tensile (OHT) is demonstrated and compared to the experimental reference [22]. The detailed methodology of the numerical tool and the relevant material models are discussed in Section 2. The simulation models for calibration and demonstration are described in Section 3. The analysis results are discussed in Section 4, followed by the conclusions in Section 5.

2. NUMERICAL METHOD

2.1 Quasi-3D XFEM

The CZM-XFEM framework employed in this paper is originally proposed by Nagashima and Sawada, utilizing a level-set based method as illustrated in Figure 1. Cohesive elements are used to model delamination on the interfaces, while the quasi-3D XFEM is employed to describe intralaminar cracks. In the quasi-3D XFEM, in-ply cracks are represented on a 2D-based mesh using level set functions. Subsequently, a quasi-3D model is extruded along the thickness direction. For elements containing cracks, a discontinuous function is introduced to enrich the nodes and elements, enabling the modeling of the discontinuous displacement field. Further details of the numerical framework can be found in [20, 21].

2.2 Constitutive model of CZM

In this paper, Geubelle and Taylor's model [7] is applied for describing the damage in the numerical models. A damage variable *D* is defined and used in the traction-separation relationship:

$$\tau_i = \frac{(1-D)}{D}\frac{\tau_{iC}}{\delta_{iC}}\delta_i \tag{1}$$

where τ_{iC} and δ_{iC} are cohesive strengths and critical relative displacements in I and II fracture mode, respectively. *D* is calculated using the following equation:

$$D = \max\left(D_{\max}, \min\left(1, \sqrt{\left(\frac{\delta_I}{\delta_{IC}}\right)^2 + \left(\frac{\delta_{II}}{\delta_{IIC}}\right)^2}\right)\right) \tag{2}$$

where δ_I and δ_{II} represent the relative displacements in mode I and II, respectively, and $D_{\max}$ denotes the maximum *D* stored in each integration point. By utilizing the maximum function, *D* can remain monotonically increasing and cannot be reversed. Once *D* reaches 1, the integration point on the cohesive element or XFEM segment fails and separates, indicating the propagation of cracking.

2.3 Fatigue accumulation law of CZM

To model fatigue growth, we have incorporated the fatigue accumulation law developed by Okabe and Yashiro [16]. In this fatigue model, *D* is treated as a function of the number of loading cycles, *N*. As a result, the fatigue accumulation law is expressed in the form of the accumulation rate, *dD*/*dN*:

$$\frac{dD}{dN} = \alpha_m \frac{F^{\beta_m}}{(1-D)^{\gamma_m}} \tag{3}$$

where α_m, β_m and γ_m are mixed-mode fatigue parameters determined through calibration using FE models and experimental data. In the original Okabe and Yashiro's model, these parameters are obtained solely from mixed-mode experiments. However, in this study, we propose a linear interpolation equation for the mixed-mode parameters:

$$\alpha_m = \frac{\delta_I}{\delta_I+\delta_{II}}\alpha_I + \frac{\delta_{II}}{\delta_I+\delta_{II}}\alpha_{II} \tag{4}$$

where α_I and α_{II} represent α under pure mode I and II respectively. Using Eqn. 4, α_m can be determined using test data from pure mode only, allowing for a more reasonable determination of the mixed-mode parameters. Similarly, β_m and γ_m are calculated in the same manner as Eqn. 4. Additionally, a dimensionless variable of stress state, F, is introduced into Eqn. 4, considering the strengths of the CZM:

$$F = \sqrt{\left(\frac{\tau_{Imax}}{\tau_{IC}}\right)^2 + \left(\frac{\tau_{IImax}}{\tau_{IIC}}\right)^2} \tag{5}$$

where τ_{Imax} and τ_{IImax} are the maximum local cohesive stresses in mode I and II respectively, which are stored in each integration point. By utilizing the stored data arrays of local stresses and displacements, the damage rate of the cohesive zone can be calculated for each computed cycle.

2.4 Workflow of fatigue simulation

In order to minimize the computational cost of fatigue simulation, a cycle jump strategy, adapted from [15, 23], has been implemented in the numerical framework. The simulation begins at cycle number *N* = 1 utilizing an implicit static solver. The applied loading of the model is linearly increased until reaching the maximum loading. Subsequently, the increment for the next cycle, Δ*N*, is determined using the following equation:

$$\Delta N = \frac{\Delta D_{max}}{\left(\frac{dD_i}{dN}\right)_{max}} \tag{6}$$

where $\left(\frac{dD_i}{dN}\right)_{max}$ represents the maximum $\frac{dD_i}{dN}$ among all intergration points in the cohesive elements and XFEM segments. Once ΔN is determined, the array of damage variable can be updated:

$$D_i = D_{i-1} + \Delta N \left(\frac{dD_i}{dN}\right)_{i-1} \tag{7}$$

As the number of cycle increases (N > 1), the external loading applied to the simulation model remains unchanged, forming a load envelope for the core implicit solver of the CZM-XFEM framework. The same updating process will be repeated in the fatigue simulation loop until the maximum cycle number is reached. A concise flowchart of this numerical scheme is presented in Figure 2.

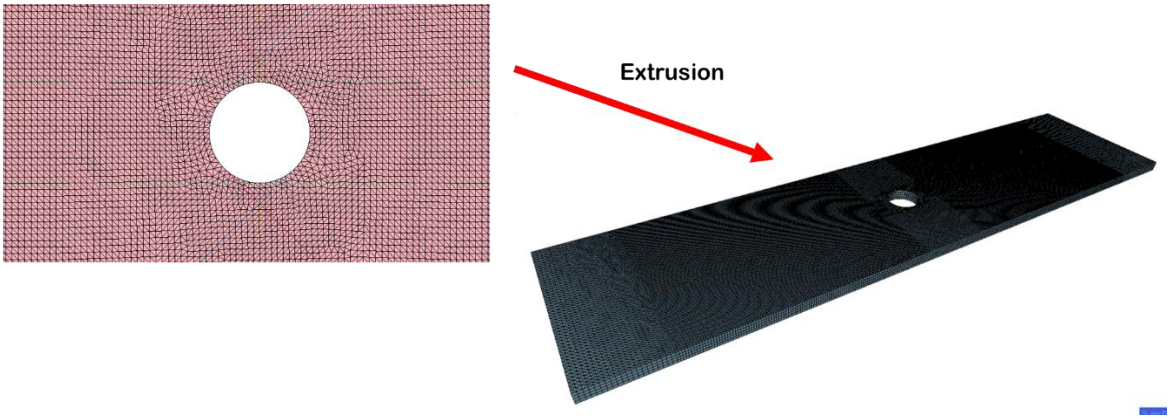

Figure 1. A scheme of modelling and extrusion process for the quasi-3D CZM-XFEM framework

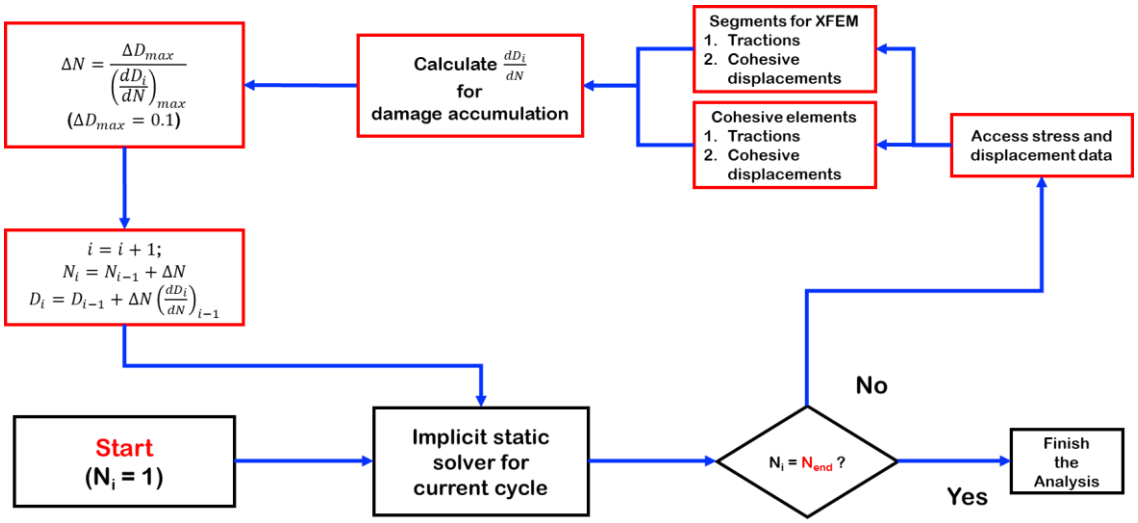

Figure 2: Flowchart of the fatigue CZM-XFEM framework.

3. SIMULATION MODELS

To demonstrate the applicability of mixed-mode loading, fatigue OHT test is chosen in the presented study. The experimental work of fatigue progression in IM7/8552 by Nixon-Pearson et. al [22] is used for the comparison of simulation results. The numerical analysis can be divided into the following steps:

1. Calibration of α_I, β_I and γ_I using DCB simulation and experimental data
2. Calibration of α_{II}, β_{II} and γ_{II} using ENF simulation and experimental data
3. Establishing fatigue OHT model with the calibrated parameters.

3.1 Calibration of mode I fatigue parameters

The experimental data from the technical report by Murri [24] was utilized for mode I calibration. The fatigue double cantilever beam (DCB) test of IM7/8552 was conducted in accordance with the standard ASTM D6115 [25]. In this study, the fatigue parameters were determined using the G-N curve, which represents the relationship between the maximum energy release rate under fatigue loading and the onset cycles of crack growth. For FE model, a static DCB simulation was initially performed to obtain the maximum displacement of the static DCB test. Then, the displacements for fatigue loading were applied at different levels of residual percentages, following the specifications of ASTM D6115. This allowed the overall G-N curve to be obtained through the FE analysis. The parameters were determined by fitting the simulation data to the experimental curve using a trial-and-error process. The material properties of unidirectional IM7/8552 for the simulations are listed in Table 1. The geometry and boundary conditions of the FE model are illustrated in Figure 3, where the fatigue DCB test model had a length of 178 mm, width of 25.4 mm, thickness of 4.5 mm, and an initial crack length of 50.8 mm. The fatigue simulation data, along with the experimental G-N curve, are presented in Figure 4. The solid line represents the fitted curve from the experimental data [24], while the dots depict the experimental results with a fitted dotted curve. Through the calibration work, the mode I parameters were identified, resulting in α_I = 0.154 and $\beta_I = \gamma_I$ = 20.65.

Table 1: Material properties of IM7/8552 [14, 21].

Properties	*Magnitudes*
E_{11}	171.0 GPa
E_{22}	9.1 GPa
G_{12}	5.3 GPa
G_{23}	3.0 GPa
v_{12}	0.32
v_{23}	0.52
G_{IC}	0.277 N/mm
G_{IIC}	0.788 N/mm
τ_{IC}	62.3 MPa
τ_{IIC}	92.3 MPa

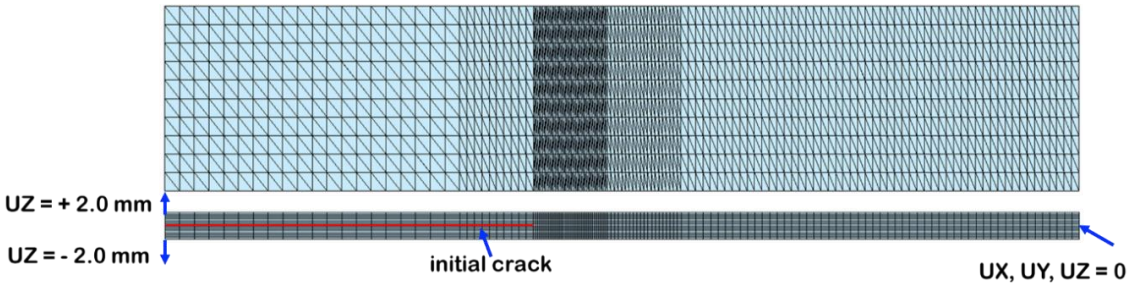

Figure 3: FE model of fatigue DCB test.

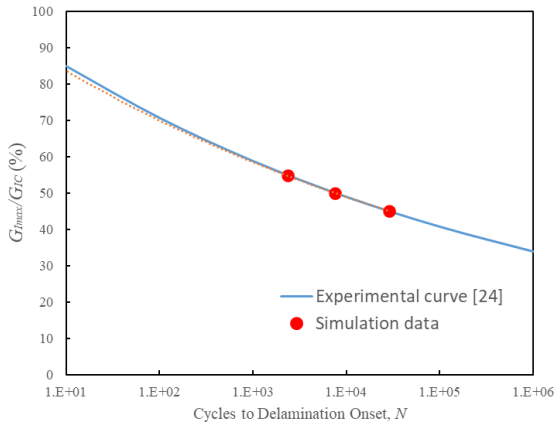

Figure 4: G-N curve of IM7/8552 under mode I loading.

3.2 Calibration of mode II fatigue parameters

The experimental data from the technical report by O'Brien et al. [26] was utilized for mode II calibration. The fatigue end-notched flexure (ENF) test of IM7/8552 was conducted, incorporating the extensions of ASTM D7905 [27] and ASTM D6115 [25], as there is no standardized mode II fatigue test. The methodology for mode II calibration followed the same process presented in Section 3.1. The geometry and boundary conditions of the FE model are illustrated in Figure 5. Using the geometry data provided in [26], the fatigue ENF test model had a length of 101.6 mm, width of 25.0 mm, thickness of 4.445 mm, and an initial crack length of 25.4 mm. The fatigue simulation data, along with the experimental G-N curve, are presented in Figure 6. The solid line represents the fitted curve from the experimental data [26], while the dots depict the experimental results with a fitted dotted curve. Through the calibration work, the mode II parameters were identified, resulting in α_{II} = 0.064 and β_{II} = γ_{II} = 10.8.

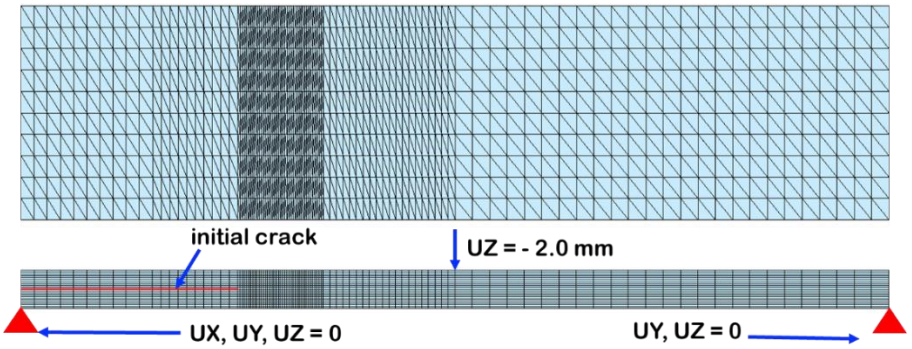

Figure 5: FE model of fatigue ENF test.

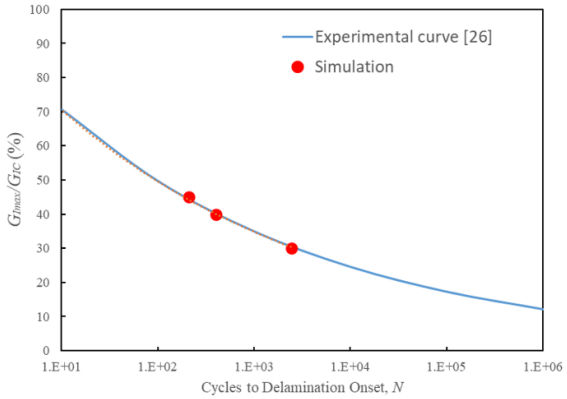

Figure 6: G-N curve of IM7/8552 under mode II loading.

3.3 Numerical model of fatigue OHT test

The FE model of the fatigue open-hole tension (OHT) test was constructed based on the experiment conducted by Nixon-Pearson et al. [22]. The stacking sequence of the OHT specimens was $[45_2/90_2/-45_2/0_2]_n$, with a nominal ply thickness of 0.125 mm. The OHT model featured a gauge length of 64 mm, thickness of 1 mm, width of 16 mm, and a hole diameter of 3.175 mm, as depicted in Figure 7. Delamination was modelled using cohesive elements, while in-ply cracking was modelled using extended finite element method (XFEM). The paths of intralaminar cracks were pre-inserted into the XFEM model based on the experimental work [22], as illustrated in Figure 8. To determine the maximum remote stress leading to static failure, a simulation of the static OHT test was performed. Following the static simulation, load-controlled fatigue simulations were conducted at 70% and 80% severity levels. A distributed load was applied to the edge of the FE model, as shown in Figure 7. Finally, the fatigue damage distribution pattern in the simulation model was compared to the experimental results.

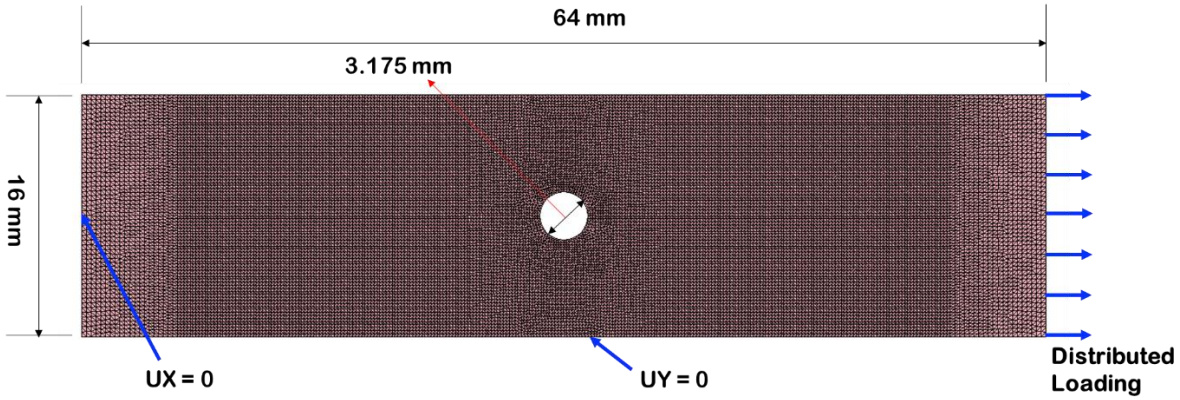

Figure 7: FE model of fatigue OHT test.

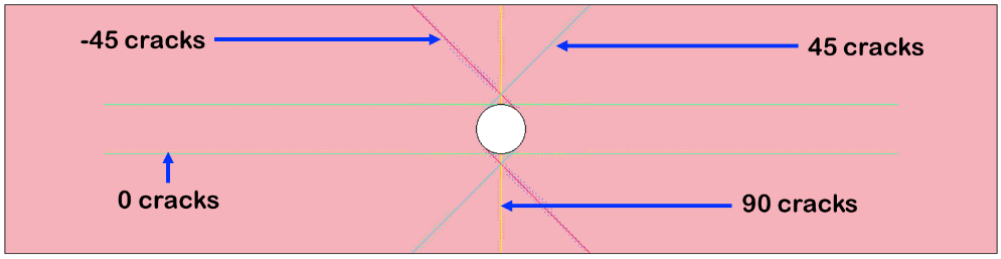

Figure 8: Pre-inserted paths of intralaminar cracks modelled by XFEM.

4. SIMULATION RESULTS AND DISCUSSIONS

The damage map from the static OHT simulation is presented in Figure 9. The static failure load obtained in the FE model is 434 MPa, which closely matches the experimental data showing failure loads of 418 MPa and 447 MPa from two different batches, respectively. Upon comparing Figure 9 with the damage initiation map from [22], it can be observed that the damage distributions exhibit similarities.

Using a nominal static failure load of 434 MPa, fatigue simulations of the OHT test were performed at severity levels of 70% and 80%. The resulting damage contours are depicted in Figure 10 and 11. As evident from these figures, the initial stages of fatigue accumulation are characterized by intralaminar cracking. Subsequently, delamination initiates at the 45/90 interface, propagating along 45° cracks, followed by delamination along 90/-45 and -45/0 interfaces. Notably, a significant drop in stiffness occurs at N = 1701 for 80% severity and N = 7985 for 70% severity. These predicted cycle numbers align with the range of experimental data [22]. Hence, the presented numerical scheme can be validated through the demonstrated example of the fatigue OHT test.

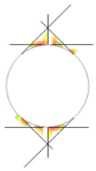

Figure 9: damage distribution ($D > 0.5$) in the FE model of static OHT test.

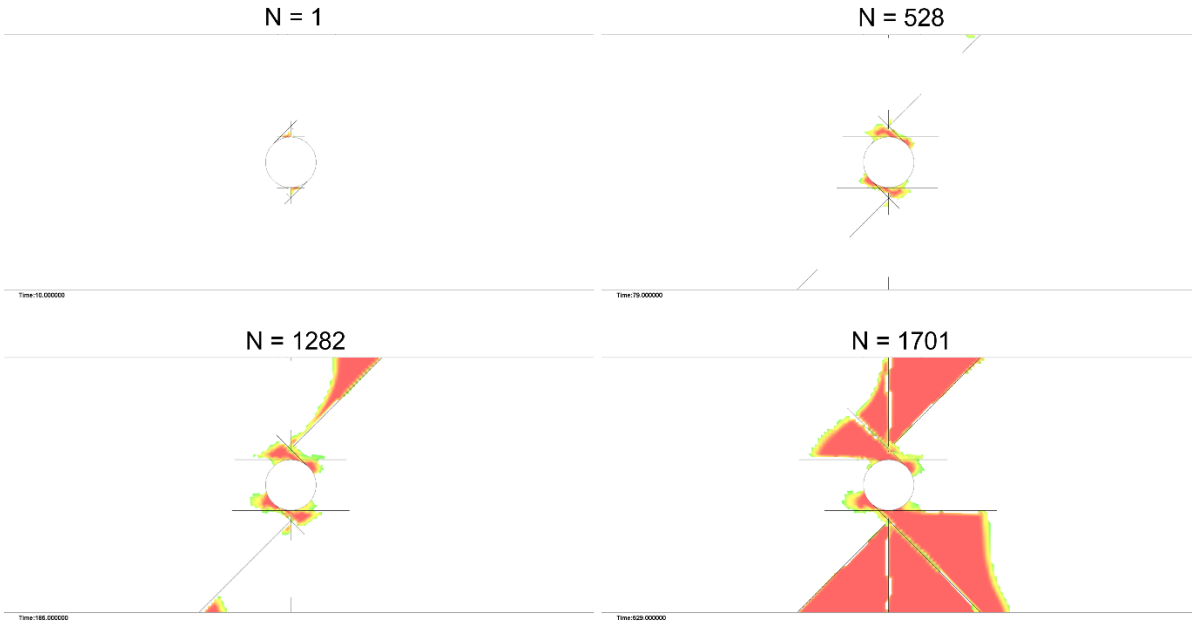

Figure 10: damage evolution in the FE model of fatigue OHT test (severity = 80%, $D \geq 0.5$).

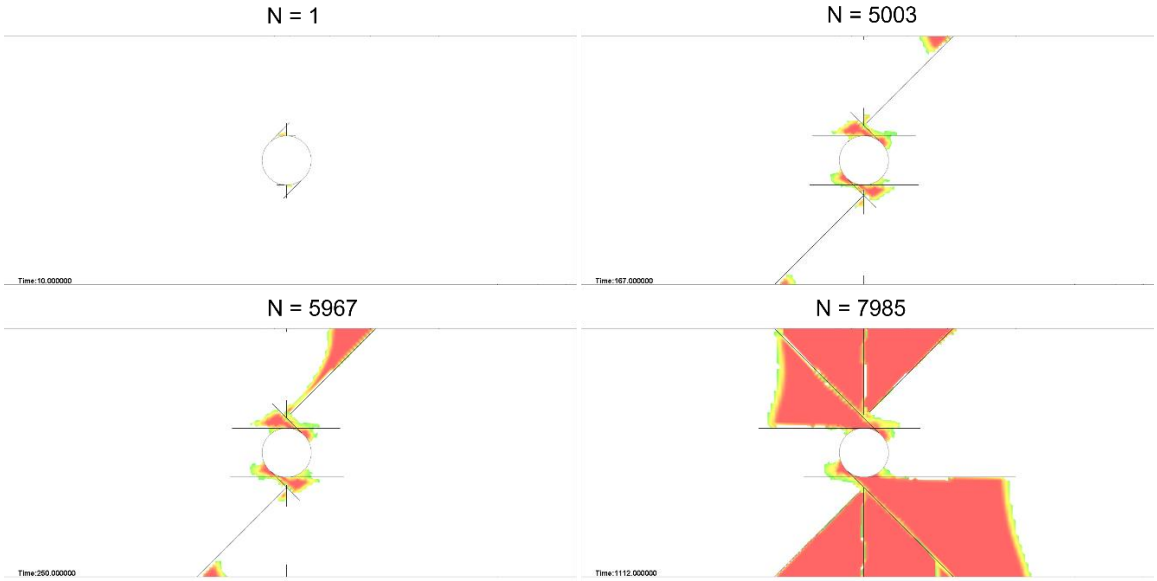

Figure 11: damage evolution in the FE model of fatigue OHT test (severity = 70%, $D \geq 0.5$).

5. CONCLUSIONS

In this paper, a numerical scheme combining cohesive elements and XFEM is proposed to predict the fatigue evolution mechanism in laminated composites. Furthermore, an extended version of the fatigue accumulation law based on Okabe and Yashiro's work [16] is introduced into the CZM-XFEM framework. The calibration methodology employed in this study allows obtaining the mixed-mode fatigue parameters from pure mode tests and utilizing the proposed interpolation equation. The extension work presented in this paper enables the application of fatigue CZM to loading cases with varying mode mixity. The CZM-XFEM scheme is validated using fatigue OHT experiments as a reference, and the detailed fatigue behaviors observed in the simulations are consistent with the experimental results [22]. By leveraging XFEM, in-ply matrix cracks can be modeled as multiple mesh-independent paths in the FE model. This paper offers a convenient and reliable approach that harnesses the capabilities of XFEM to simulate progressive fatigue damage in composite laminates.

REFERENCES

[1] Spearing, S. M. and Beaumont, P. W. R. (1992), *Compos. Sci. Technol.*, vol. 44, n. 2, pp. 159–168.
[2] Bak, B. L. V., Sarrado, C., Turon, A. and Costa, J. (2014), *Appl. Mech. Rev.*, vol. 66, n. 6.
[3] Alam, P., Mamalis, D., Robert, C., Floreani, C. and Ó Brádaigh, C. M. (2019), *Compos. B. Eng.*, vol. 166, pp. 555–579.
[4] Dugdale, D. S. (1960), *J. Mech. Phys. Solids*, vol. 8, n. 2, pp. 100–104.
[5] Barenblatt, G. (1962), *Adv. Appl. Mech.*, vol. 2, pp. 55–125.
[6] Hillerborg, A., Modeer, M., Petersson, P. E. (1976), *Cem. Concr. Res.*, vol. 6, n. 6, pp. 773–781.
[7] Geubelle, P. H. and Baylor, J. S. (1998), *Compos. B. Eng.*, vol. 29, n. 5, pp. 589–602.
[8] Camanho, P. P., Davila, C. G. and de Moura, M. F., *J. Compos. Mater.*, vol. 37, n. 16, pp. 1415–1438.
[9] Paris, P. C., Gomez, M. P. and Anderson, W. E. (1961), *Trend Eng.*, vol. 13, n. 1, pp. 9–14.
[10] Ramkumar, R. L. and Whitcomb, J. D. (1985). In: *Delamination and Debonding of Materials, ASTM STP 876*, pp. 315-335, American Society for Testing and Materials, Philadelphia.
[11] Dahlem, C. and Springer, G. (1994), *J. Compos. Mater.*, vol. 28 n. 8, pp. 732–781.
[12] Robinson, P., Galvanetto, U., Tumino, D., Bellucci, G. and Violeau, D. (2005), *Int. J. Numer. Methods Eng.*, vol. 63, n. 13, pp.1824–1848.
[13] Turon, A., Costa, J., Camanho, P. P. and Dávila, C. G. (2007), *Compos. Part A Appl. Sci. Manuf.*, vol. 38, n. 11, pp. 2270–2282.
[14] Harper, P. W. and Hallett, S. R. (2010), *Int. J. Fatigue*, vol. 32, n. 11, pp. 1774–1787.
[15] Nojavan, S., Schesser, D. and Yang, Q. D. (2016), *Compos. Struct.*, vol. 146, pp. 34–49.
[16] Okabe, T. and Yashiro, S. (2009), *J. Solid. Mech. Mater. Eng.*, vol. 3, pp. 1202–1211.
[17] Belytschko, T. and Black, T. (1995), *Int. J. Numer. Meth. Eng.*, vol. 45, n. 5, pp. 605–620.
[18] Moës, N., Dolbow, J. and Belytschko, T. (1999), *Int. J. Numer. Meth. Eng.*, vol. 46 n. 1, pp. 131–150.
[19] Moës, N. and Belytschko, T. (2002), *Eng. Fract. Mech.*, vol. 69, n. 7, pp. 813–833.
[20] Nagashima, T. and Sawada, M. (2016), Comput. Struct., vol. 174, pp. 42–53.
[21] Higuchi, R., Okabe, T. and Nagashima T. (2017), *Compos. Part A Appl. Sci. Manuf.*, vol. 95, pp. 197–207.
[22] Nixon-Pearson, O., Hallett, S. R., Withers, P. J., Rouse, J. (2013), Compos. Struct., vol. 106, pp. 882–889.
[23] Van Paepegem, W. and Degrieck, J. (2001), *Compos. Part A Appl. Sci. Manuf.*, vol. 32, pp. 1433–1441.
[24] Murri, G. B. (2013). In: *Evaluation of Delamination Onset and Growth Characterization Methods under Mode I Fatigue Loading, NASA/TM-2013-217966*, National Aeronautics and Space Administration, USA.
[25] American Society for Testing and Materials (2011). In: *ASTM D6115-97: Standard Test Method for Mode I Fatigue Delamination Growth Onset of Unidirectional Fiber-Reinforced Polymer Matrix Composites*, American Society for Testing and Materials, ASTM international, USA.

[26] O'Brien, T. K., Johnston, W. M. and Toland, G. J. (2010). In: *Mode II Interlaminar Fracture Toughness and Fatigue Characterization of a Graphite Epoxy Composite Material, NF1676L-10105*, National Aeronautics and Space Administration, USA.
[27] American Society for Testing and Materials (2011). In: *ASTM D7905-14, Standard Test Method for Determination of the Mode II Interlaminar Fracutre Toughness of Unidirectional Fiber-Reinforced Polymer Matrix Composites*, American Society for Testing and Materials, ASTM international, USA.